Southeastern Tibetan Plateau Growth Revealed by Inverse Analysis of Landscape Evolution Model

X. Yuan, R. Jiao, Guillaume Dupont-Nivet, X. Shen

AGU ADVANCING EARTH AND SPACE SCIENCE

Geophysical Research Letters®

RESEARCH LETTER
10.1029/2021GL097623

Southeastern Tibetan Plateau Growth Revealed by Inverse Analysis of Landscape Evolution Model

X. P. Yuan[1], R. Jiao[2], G. Dupont-Nivet[3,4], and X. Shen[5]

[1]Hubei Key Laboratory of Critical Zone Evolution, School of Earth Sciences, China University of Geosciences, Wuhan, China, [2]School of Earth and Ocean Sciences, University of Victoria, Victoria, BC, Canada, [3]Géosciences Rennes-UMR CNRS 6118, University of Rennes 1, Rennes, France, [4]Institute of Geosciences, Potsdam University, Potsdam, Germany, [5]National Institute of Natural Hazards, Ministry of Emergency Management of China, Beijing, China

Abstract The Cenozoic history of the Tibetan Plateau topography is critical for understanding the evolution of the Indian-Eurasian collision, climate, and biodiversity. However, the long-term growth and landscape evolution of the Tibetan Plateau remain ambiguous, it remains unclear if plateau uplift occurred soon after the India-Asia collision in the Paleogene (~50–25 Ma) or later in the Neogene (~20–5 Ma). Here, we reproduce the uplift history of the southeastern Tibetan Plateau using a 2D landscape evolution model, which simultaneously solves fluvial erosion and sediment transport processes in the drainage basins of the Three Rivers region (Yangtze, Mekong, and Salween Rivers). Our model was optimized through a formal inverse analysis with 20,000 forward simulations, which aims to reconcile the transient states of the present-day river profiles. The results, compared to existing paleoelevation and thermochronologic data, suggest initially low elevations (~300–500 m) during the Paleogene, followed by a gradual southeastward propagation of topographic uplift of the plateau margin.

Plain Language Summary When and how was formed the Tibetan Plateau which includes the highest mountains in the world? The answer is critical to decipher between competing models trying to explain how the Indian and Asian tectonic plates behaved when they collided. It is also a major constraint on the evolution of Asian mountain biodiversity, Asian monsoons, and even global climate. However, current estimates of past Tibetan elevation are contradictory, some arguing for a high plateau since the onset of the India-Asia collision over 50 million years ago, while others favor the region remained low until a sudden rise 25 million years ago. Here, we use a numerical model of landscape evolution to test various hypothesis focusing on the southeastern Tibetan Plateau. We compared the results to see how they fit with the observed river profiles of the Three Rivers. The best fits were obtained with low elevations between 50 and 25 million years ago, and a more gradual growth toward the southeast of the high-elevated plateau until present day.

Key Points:

- We constrained the uplift history of the southeastern (SE) Tibetan Plateau by performing inversion of the Three Rivers profiles
- The inversion suggests that SE Tibet was at a low elevation until 50–25 Ma, followed by gradual outward growth until 0 Ma
- Our modeling does not support Paleogene formation of the SE Tibetan Plateau with a major subsequent degradation via upstream fluvial erosion

Supporting Information:

Supporting Information may be found in the online version of this article.

Correspondence to:

X. P. Yuan,
yuanxiaoping@cug.edu.cn;
xyuan@gfz-potsdam.de

Citation:

Yuan, X. P., Jiao, R., Dupont-Nivet, G., & Shen, X. (2022). Southeastern Tibetan Plateau growth revealed by inverse analysis of landscape evolution model. *Geophysical Research Letters*, *49*, e2021GL097623. https://doi.org/10.1029/2021GL097623

Received 23 JAN 2022
Accepted 29 APR 2022

Author Contributions:

Conceptualization: X. P. Yuan, G. Dupont-Nivet
Formal analysis: X. P. Yuan, R. Jiao, X. Shen
Funding acquisition: X. P. Yuan
Methodology: X. P. Yuan
Validation: X. P. Yuan, R. Jiao, G. Dupont-Nivet, X. Shen
Writing – original draft: X. P. Yuan
Writing – review & editing: R. Jiao, G. Dupont-Nivet, X. Shen

1. Introduction

A well-constrained paleotopographic history of the Tibetan Plateau is lacking to assess competing geodynamic models of India-Eurasian collision and estimate associated plateau growth interactions with Asian climate (Botsyun et al., 2019; Fang et al., 2020; Zhao et al., 2021). The world's highest mountains represent a natural laboratory to constrain models that link topography, geodynamic processes, drainages, biodiversity, and climate (Deng & Ding, 2015). Major questions include the timing and configuration of the India-Asia collision (Bouilhol et al., 2013), plateau growth mechanisms involving lithospheric thickening, delamination, lower crustal flow or surface processes with (or without) interactions between climate and orogeny (e.g., Molnar et al., 2015; Royden et al., 2008; Tapponnier et al., 2001; Yuan et al., 2021), the potential role of the orogen as a major sink of the global carbon cycle (Märki et al., 2021), and the orogen as a cradle, museum, or abiotic driver of biodiversity hotspots when combined with flickering climate trends (Favre et al., 2015).

Recently, paleoelevation data have been obtained in the region from a wide range of innovative techniques. In the sedimentary archives, fossil content including pollen, plant remains, leaf, fish, and mammal physiognomies were recovered (Spicer et al., 2021), and stable-isotope palaeoaltimetry was applied to pedogenic carbonates and biomarkers (Quade et al., 2020). Despite these many efforts to estimate the Cenozoic paleotopography of the Tibetan Plateau, widely different topographic growth scenarios have been proposed, from a high plateau (or "Lhasaplano") prior to the onset of the India-Asia collision (Kapp & DeCelles, 2019; Rowley & Currie, 2006), to

a much more recent mostly Neogene uplift and the preservation of broad low-elevation valleys until the Miocene (Spicer et al., 2021; Wei et al., 2016).

In SE Tibet, there are two end-member models to explain the plateau uplift. The late uplift models (Figure 1d) suggest that the modern topography is resulted from crustal thickening due to ongoing lower crustal flow mainly since the middle Miocene (Clark & Royden, 2000; Royden et al., 2008). In contrast, early uplift models (Figure 1e) indicate that the SE Tibetan Plateau had attained its present elevation long before the middle Miocene or the Oligocene (Tapponnier et al., 2001), as a result of thickening and extrusion along large strike-slip faults at the onset of the collision (e.g., Leloup et al., 1995; Replumaz & Tapponnier, 2003). The early uplift models often imply that the plateau margin underwent later relief reduction and retreat due to upstream fluvial erosion (Groves et al., 2020).

Here, we investigate the long-term formation history of the high topography on the SE Tibetan Plateau using a numerical landscape evolution model (Yuan et al., 2019). We specifically test three questions related to the above scenarios: (a) Did the regional elevation start low or high as a pre-existing plateau? (b) When did plateau growth occur, and was it gradual or fast within a short uplift phase? (c) Has the uplifted plateau experienced subsequent degradation or has plateau growth continued to the present day?

As the landscape evolution is controlled mainly by mountain uplift and surface processes, the present-day river profiles and the drainage basin geometries preserve important information that can be extracted to infer the long-term history of mountain uplift with numerical models (e.g., Goren et al., 2014; Roberts & White, 2010). We focus on the SE Tibetan Plateau where three of the world's largest rivers draining the Tibetan Plateau (the Yangtze, Mekong, and Salween Rivers, i.e., Three Rivers) have incised deep valleys with distinctive geomorphic signatures (Figures 1a and 1b). Modeling shows that drainage networks are substantially varying throughout landscape evolution in SE Tibet (Yuan et al., 2021), which suggests that the modeling assumption of time-invariant drainage area (e.g., Goren et al., 2014; Roberts & White, 2010) may not be applicable to this area. We constrained a set of model parameters that best fit the current transient states of the long profiles of these rivers, using a large number of forward process simulations. Our modeling results were ultimately compared to existing thermochronologic and paleoelevation data sets to help decipher between competing tectonic models that predict contrasting topographic evolutions.

2. Methods

2.1. Landscape Evolution Model and Model Setup

We used FastScape landscape evolution model (Text S1.1 in Supporting Information S1; Yuan et al., 2019, 2022) to simulate the fluvial erosion and sediment deposition processes in the drainage basins of the Three Rivers region, with boundary conditions set by crustal shortening (Text S1.2 in Supporting Information S1) and tectonic uplift rates (Section 2.2 and Text S1.3 in Supporting Information S1). We defined an initial rectangular domain size of 1,300 × 500 km (Figure 1g) with each cell size of 2 × 2 km, and the model runs from the initial growth age t_i to the final growth age t_f of SE Tibet with a time step length of 10,000 years. We assumed an initial elevation h_0 of SE Tibet and a random ≤100-m amplitude white noise in our modeling.

2.2. Propagating Uplift of Plateau Growth

In our initial setup, we used a simple assumption that mountain belts grow first to a certain height and then expand laterally in an outward propagation sequence characterized by successive marginal uplift, as described by various geodynamic models (e.g., Jammes & Huismans, 2012; Wolf et al., 2021). Based on the outward plateau growth model and the present-day (low-relief) maximum topography of SE Tibet (Figure 1f), we prescribed a propagating uplift function (Text S1.3 in Supporting Information S1) to the landscape evolution model. The propagating uplift function (Equation S1.7 in Supporting Information S1) with several free parameters allows to simulate various uplift cases that predict different topographic evolutions. The unknown model parameters are the erodibility K_f (Text S1.1 in Supporting Information S1), the initial elevation h_0, the initial and final growth ages t_i and t_f of the plateau, and the width W of the plateau margin.

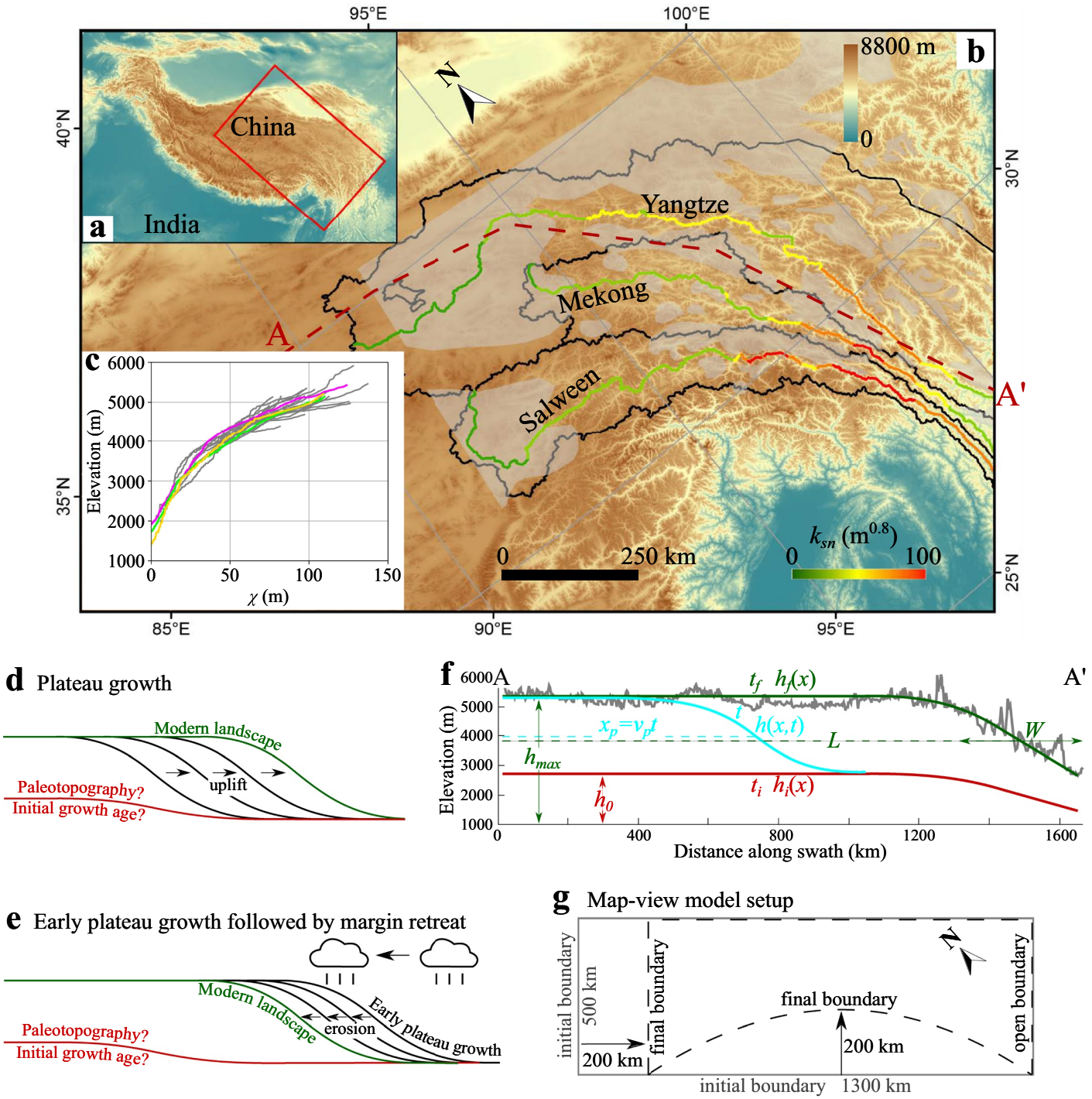

Figure 1. The study area in the Tibetan Plateau. (a) Map of the Tibetan Plateau. (b) Closer view of the study area with the high-elevation, low-relief surfaces (gray shading; Clark et al., 2006). Trunk channels of the Three Rivers are colored with the channel steepness $k_{sn} = SA^{m/n}$ with $m/n = 0.4$ (Yuan et al., 2021). (c) χ-elevation plot (Equation 1) (yellow: Salween; green: Mekong; magenta: Yangtze; gray: tributaries of the Three Rivers). Two competing models: (d) plateau growth and (e) early plateau growth followed by margin retreat, modified from Groves et al. (2020). (f) Present-day maximum topography (gray curve; Whipple et al., 2017) used to reconstruct the plateau uplift. The location of A–A′ is shown in (b). Red, cyan, and green curves represent the topographies ($h_i(x)$, $h(x,t)$, and $h_f(x)$) at the initial growth age t_i, the timing t, and the final growth age t_f, respectively (see Text S1.3 in Supporting Information S1 for details). (g) Model setup with initial (gray) and final (black dashed) boundaries (see Text S1.2 in Supporting Information S1 for details).

2.3. Inverse Analysis and Misfit Function

We used the inverse analysis of landscape evolution model to explore the multidimensional space of free parameters (K_f, h_0, t_i, t_f, and W), searching for optimum values that produce modeling results best matching the observed river long profiles in the area. To normalize river profiles, a parameter χ (Perron & Royden, 2013) was computed by integration of drainage area along the river profile from base level x_b to a point x as

$$\chi(x) = \int_{x_b}^{x} \left(\frac{A_0}{A(x)} \right)^{m/n} dx, \tag{1}$$

where A_0 (=1 m^2) is a reference drainage area. We used $m = 0.4$ and $n = 1$, based on the concavity $m/n = 0.4$ that minimizes scatter between the observed χ-elevation profiles of tributary profiles in the Three Rivers basins (Figure 1c; Yuan et al., 2021). Several cases with non-linearity $n \neq 1$ are shown in Text S4 in Supporting Information S1.

We calculated the average observed χ_i^{obs} values of the Three Rivers at each elevation bin h_i ($i = 1, 2, \ldots, N_\chi = 200$), with N_χ the number of evenly spaced elevation bins. At the end of each model run, we identified the three largest rivers draining across the entire model domain, and calculated the average simulated χ_i^{sim} values at each elevation bin h_i for the rivers. To compare the modeled and observed river profiles, we defined a misfit function as

$$\mu = \sqrt{\frac{1}{N_\chi} \sum_{i=1}^{N_\chi} \frac{\left(\chi_i^{obs} - \chi_i^{sim}\right)^2}{\left(\delta_\chi\right)^2}}, \tag{2}$$

where δ_χ is the uncertainty for the χ comparison which we arbitrarily set at 8 m.

We performed the inverse analysis to constrain five parameters (K_f, h_0, t_i, t_f, and W) in their respective ranges: (a) the erodibility K_f in the range of 1×10^{-7}–5×10^{-6} m$^{0.2}$/yr, (b) the initial elevation h_0 in the range of 0–4,000 m, including the ranges of the plateau in the Eocene (Ding et al., 2014; Hetzel et al., 2011; Rowley & Currie, 2006; Su et al., 2019, 2020), (c) the initial growth age t_i = 50–20 Ma, including the synthesized low-temperature thermochronologic ages of 50-30 Ma from the headwaters and interfluves of the deep valleys of the Three Rivers (Li et al., 2019; Figure S1 in Supporting Information S1), (d) the final growth age t_f = 20-0 Ma, including possible final growth ages to its maximum topography (Clark et al., 2005; Liu-Zeng et al., 2008), and (e) the characteristic width W = 100–300 km of the propagating zone of uplift. These parameters were explored to minimize the misfit function in Equation 2, using the Neighborhood Algorithm (Sambridge, 1999). A total of 20,000 simulations (40 iterations, with 500 simulations per iteration and 60% resampling rate) were performed to explore the parameter space. In the next section, we first show the results of the inverse analysis, and then use two sets of numerical experiments to explore the pre-existing plateau scenario and the topographic degradation scenario.

3. Results

The optimization converges to a range of parameters predicting the observed data within uncertainty, i.e., misfit values $\mu < 1$ or $log_{10}(\mu) < 0$ (Figures 2a–2c). The minimum misfit values are obtained for the initial growth age t_i = 50–25 Ma and the erodibility $K_f = (1.2\text{–}2.4) \times 10^{-6}$ m$^{0.2}$/yr (Figure 2a and Figure S2 in Supporting Information S1), the initial low elevation h_0 = ~300–500 m of SE Tibet and the final growth age t_f = 0–3 Ma to its maximum topography (Figure 2b), and a characteristic width W = 150–170 km of the propagating zone of uplift (Figure 2c). The narrow range of best-fit values for W is consistent with the estimate of W = 150 km based on the swath profiles across the SE plateau margin (Yuan et al., 2021). The initial growth ages t_i and erodibilities K_f are in a relatively large range (Figure 2a), with younger ages t_i (thus faster plateau growth based on the relationship between t_i and t_f in Figures S2 and S3 in Supporting Information S1) corresponding to larger K_f (thus weaker rock) to form the observed river profiles. Note that it is unlikely to use a well constrained K_f for further constraining the value of t_i, because the K_f value is highly variable within the range of 10^{-7}–10^{-4} m$^{0.2}$/yr (Stock & Montgomery, 1999) and is dependent much on rainfall, lithology, fracturation, and vegetation cover (Whipple & Tucker, 1999). For cases of $n \neq 1$ (Text S4 and Figures S8–S10 in Supporting Information S1), there are some trade-offs between K_f and n (Goren et al., 2014). The potential variation of n could add ~20% uncertainty to our estimate of initial growth age t_i. The other main results remain similar when using different n values: (a) the

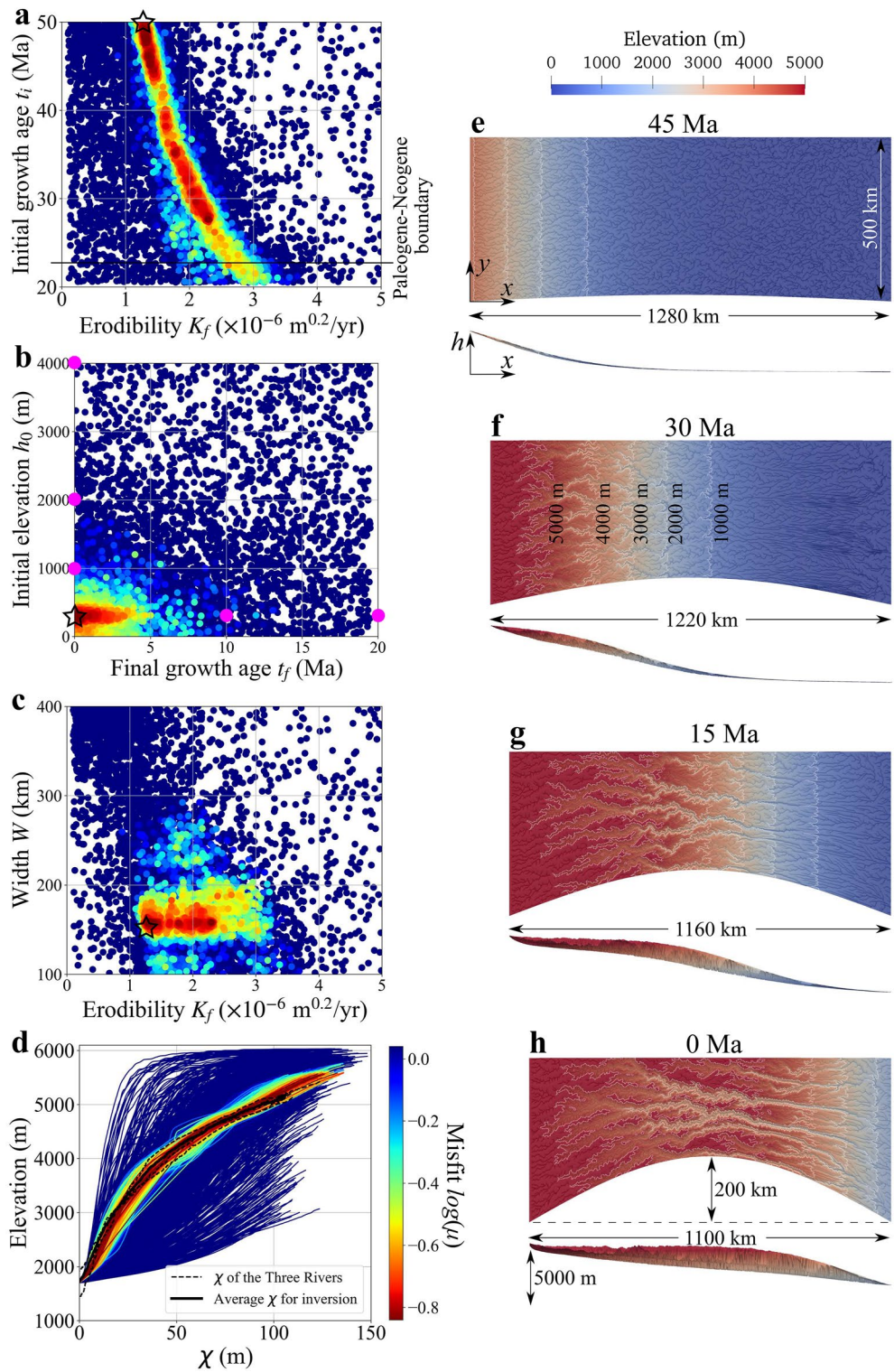

Figure 2. The inverse analysis (left panel) and one of the best-fit modeling results (right panel). (a) Inverse results for the erodibility K_f and the initial growth age t_i. (b) Results for the final growth age t_f and initial elevation h_0. (c) Results for K_f and the characteristic width W. The full parameter correlation is shown in Figure S2 in Supporting Information S1. (d) Comparison of the modeled and observe χ-elevation plot. (e–h) The landscape evolution of simulation at 45, 30, 15, and 0 Ma, respectively, using one set of optimum parameters ($K_f = 1.2 \times 10^{-6}$ m$^{0.2}$/yr, $h_0 = 300$ m, $t_i = 50$ Ma, $t_f = 0$ Ma, $W = 150$ km; stars on panels (a–c); Movie S1 in Supporting Information S1). Magenta dots in (b) indicate the poor-fitting parts of parameter space with their river profiles shown in Figures 3a–3c, and 3e, 3f.

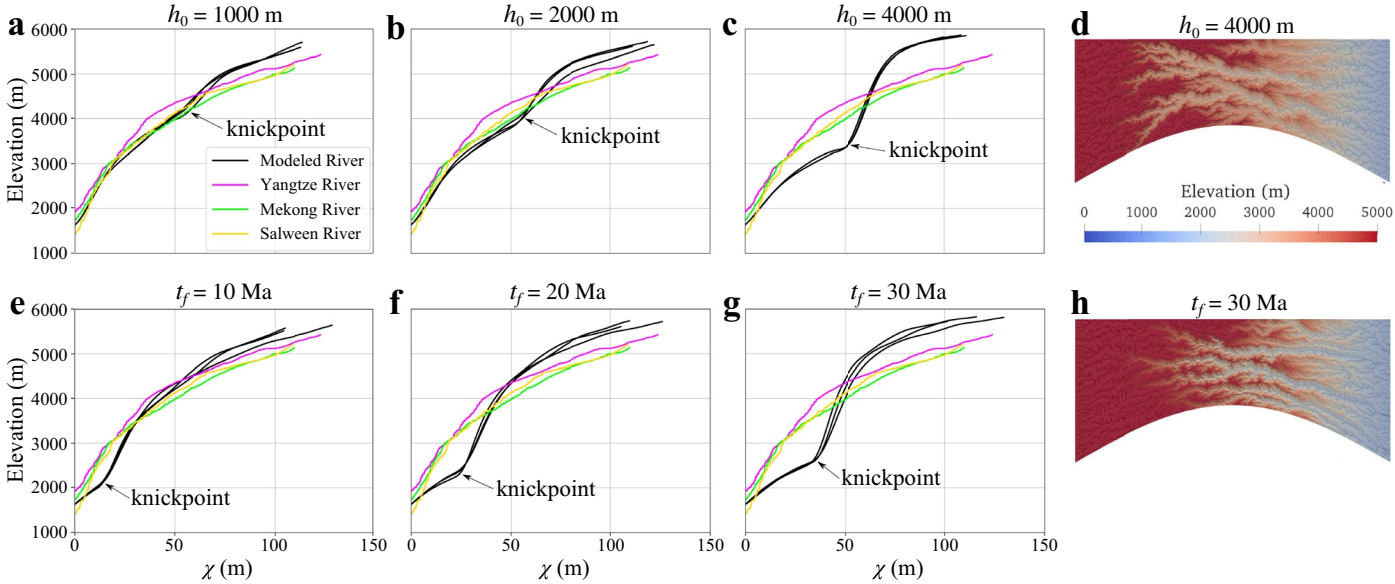

Figure 3. χ-elevation plots of river profiles of the three largest rivers at the end of landscape evolution for various initial elevations h_0 and final growth ages t_f, using the initial growth age $t_i = 50$ Ma, the erodibility $K_f = 1.2 \times 10^{-6}$ m$^{0.2}$/yr and the width $W = 150$ km. (a–c) χ-elevation plot for the cases of h_0 = 1,000, 2,000, and 4,000 m, respectively, using a constant final growth age $t_f = 0$ Ma. (d) Landscape at 0 Ma for the case of $h_0 = 4{,}000$ m (Figure S4 and Movie S2 in Supporting Information S1). (e–g) χ-elevation plot for the cases of t_f = 10, 20, and 30 Ma, respectively, using a constant initial elevation $h_0 = 300$ m. (h) Landscape at 0 Ma for the case of $t_f = 30$ Ma (Figure S5 and Movie S3in Supporting Information S1).

initial elevation h_0 is low; (b) the initial growth age t_i is in a relatively large range; and (c) the final growth age t_f is relatively late. In the following, we focus our discussion based on results using $n = 1$.

The modeled χ-elevation profiles of the best-fit modeling results are consistent well with the observed ones (Figure 2d). Our best-fit model shows that the initial propagating uplift forms elongated drainage basins at the front of tilted propagating margin (Figures 2e, 2f, and 4a; Movie S1 in Supporting Information S1). The elongated drainage basins extend downstream during ensuing uplift propagation (Figure 2g). The modeled landscape is finally characterized with widespread low-relief surfaces in the headwaters and the interfluves of deep valleys in the propagating margin (Figures 2h and 4b; Yuan et al., 2021). The low-relief surfaces in the high-elevation plateau are coplanar and decrease progressively in elevation across the plateau margin toward the southeast, consistent with the observations (Whipple et al., 2017; Yuan et al., 2021).

To explore initial setups consistent with the pre-existing plateau scenario, we investigated the impact of having a higher plateau at the beginning of the model, and produced the landscapes and χ-elevation plots for the cases of h_0 = 1,000, 2,000, and 4,000 m. Under such settings, the knickpoints of river profiles are predicted to locate relatively far from the SE plateau margin (Figures 3a–3c). Contrasting to the observed features in the SE Tibetan Plateau, the modeled landscape characteristics of these cases show a general lack of low-relief surfaces and deep, narrow valleys in the plateau margin (Figures 3d, 4c; Figure S4 and Movie S2 in Supporting Information S1). This is because, for an initial high plateau elevation h_0 and an associated low amplitude of later uplift ($h_{max} - h_0$) in Equation S1.7 in Supporting Information S1, the plateau margin has been subject to upstream propagation of river erosion and valley widening for a long time.

Similarly, to explore the possibilities of topographic degradation since the end of plateau growth, we show the impact of different final growth age t_f, using several simulations with various t_f, e.g., 10, 20, and 30 Ma (Figure 3h; Figure S5 and Movie S3 in Supporting Information S1), under a constant initial growth age $t_i = 50$ Ma. For these cases, the plateau experienced growth from t_i to the final growth age t_f, from t_f to the present day (0 Ma) the plateau margin underwent retreat via upstream fluvial incision. The modeled χ-elevation plots for these cases show significant discrepancy with the observations (Figures 3e–3g). Due to a longer time of upstream propagation of erosion and retreat of the plateau margin, the knickpoints of rivers are located relatively far away from the plateau margin. The modeled retreat distances are consistent with analytical solution (Text S2 and Figure S6 in Supporting Information S1).

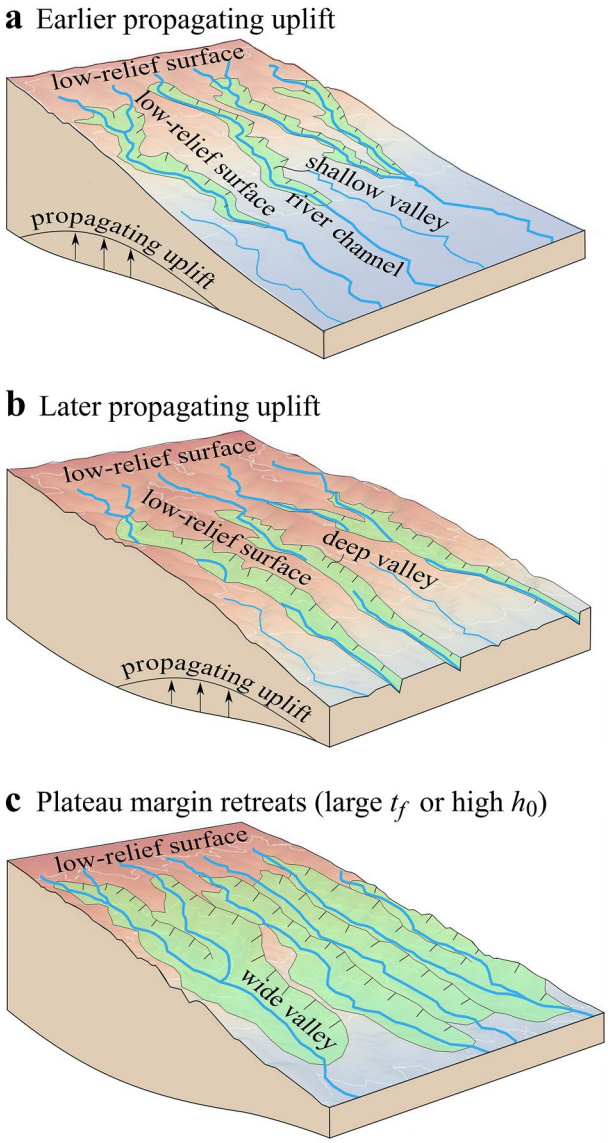

Figure 4. Cartons showing the patterns of river erosion in response to propagating uplift and plateau margin retreat. (a) The initial propagating uplift forms elongated drainage basins at the front of propagating margin, and low-relief surfaces exist in the headwater and interfluves of mainstem rivers. (b) The elongated basin extended downstream during the uplift propagating forward, forming deep valleys at the propagating margin. (c) For early plateau growth (large t_f) or initially high plateau elevation h_0, rivers undergo a major upstream erosion, and the plateau margin retreats with widening valleys.

4. Discussion

4.1. Paleogene Growth Onset With Low Elevations

Using the inverse analysis, we show that SE Tibet started growing from an initially low elevation of ~300–500 m (Figure 2b) within an initial growth age range t_i = 50–25 Ma (Figure 2a). The range of initial growth age is generally consistent with most of the exhumation ages of 50−30 Ma on the headwaters and interfluves of the Three Rivers (Figure S1 in Supporting Information S1; Li et al., 2019) and the activation of SE extruding strike-slip faults around 40–30 Ma (e.g., Replumaz & Tapponnier, 2003).

The implied timing of plateau growth onset from low elevation is consistent with previous studies showing that the headwaters of the Three Rivers in central Tibet initiated from a low-elevation basin bounded by the Gangdese and Qiangtang mountains during the Eocene (Ding et al., 2014; Fang et al., 2020; Xiong et al., 2020, 2022) and that the basins hosted large lake systems in the middle Paleogene (Spicer et al., 2021; Su et al., 2020). Our results showing low Paleogene elevations are thus also consistent with the inference of low elevations in central Tibet Gerze Basin (northern Lhasa terrane) during the late Eocene based on foraminifera recovered from deposits and oxygen-isotope data (Wei et al., 2016), as well as fossil-based low Paleogene elevations estimated in the Bangor Basin of central Tibet (Su et al., 2020). Yet, in basins located in the northern Lhasa terrane at approximately the same latitude as the Gerze Basin, paleoelevation studies show that, by the late Oligocene (~26 Ma), the Nima Basin had reached 4,500–5,000 m (DeCelles et al., 2007) and the Lunpola Basin had reached 4,000 ± 500 m (Fang et al., 2020). These results indicate that the northern Lhasa terrane (central Tibet) experienced surface uplift to ~4,000 m from the (late) Eocene to the late Oligocene. Our modeling also suggests that the central part of the plateau grew rapidly, vertically from low elevation to high elevation (Figures 2e and 2f), prior to the southeastward propagation of the plateau margin. In contrast, previous studies using stable-isotope paleoaltimetry data suggest that the SE plateau margin (Yunnan) reached its present-day elevation of ~3.3 km in the late Eocene (Hoke et al., 2014), and the plateau margin (Jianchuan Basin) was near its present-day elevation (~2.6 km) by ~40 Ma (Li, Currie et al., 2015). However, Gourbet et al. (2017) subsequently reevaluated the same data in the Jianchuan Basin and estimated lower elevations of ~1.2 ± 1.2 km, which is consistent with our modeling results that predict a low topography of the plateau margin at that time.

4.2. Gradual Propagating Uplift Without Major Subsequent Degradation

The relatively late t_f and long $t_i - t_f$ constrained by our models (Figure S3 in Supporting Information S1) imply that a gradual, outward propagation of the plateau continued until the present day (t_f = 0 Ma; Figure 2b), for any optimum initial growth age t_i (50–25 Ma) and initial elevation h_0. An earlier formation of the plateau, implemented by a faster propagation of the plateau ending earlier, is not supported by the modeled landscape of the plateau margin that is then subject to a degradation phase, because the plateau degradation results in much wider river channels with knickpoints that propagated upstream much further away from the plateau margin compared to observed river profiles (Figures 3e–3h, 4c; Figure S5 and Movie S3 in Supporting Information S1). Thus, based on the transience of the river profile and the geomorphic features of drainage basins of our modeling, we favor a simple growth model of the plateau margin with principally ongoing outward propagation of the uplift zone, and

do not suggest early formation of plateau with a major subsequent degradation phase (Tapponnier et al., 2001). The ongoing outward propagation can be balanced by surface erosion since the late Miocene (Shen et al., 2022).

The ongoing propagation model of the plateau margin ($t_f = 0$ Ma) is consistent with the continuous expansion of high topography in the SE plateau margin (Clark & Royden, 2000). Moreover, our modeling suggests a simple, gradual uplift from the central plateau since the Paleogene rather than a late-stage uplift propagation in the eastern margin since the middle Miocene (Royden et al., 2008). A progressive southeastward growth from the central plateau since the Paleogene is in agreement with synthesized structural analyses (Li, Wang et al., 2015; Wang et al., 2014) and compiled thermochronologic ages (Li et al., 2019; Figure S1 in Supporting Information S1), showing a younging trend from the central plateau (with almost exclusively Paleogene ages) to the SE plateau margin (with ages extending up to the Pliocene). Our modeling results, showing gradual propagation rather than initial wholesale uplift (e.g., for $t_f \approx 20$ Ma and $t_i - t_f \approx 0$ in Figure S3 in Supporting Information S1) in SE Tibet, are also consistent with various geodynamic models which suggest that the plateau expanded progressively in an outward propagation sequence characterized by successive marginal uplift (e.g., Penney & Copley, 2021; Wolf et al., 2021). This outward propagation with deeply incised valleys is also consistent with the early Oligocene diversification of Alpine flora linked to joint uplift and monsoonal intensification in central Tibet (Ding et al., 2020), followed by the late Miocene development of SE Tibet biodiversity hotspots (e.g., the Hengduan mountains) that have been genetically linked to orogenesis and habitat segmentation by incising drainages (e.g., Xing & Ree, 2017).

Our modeling results were obtained based on a propagating uplift function, which is likely the simplest plausible one. However, this simple model does not take into account complexities of SE Tibet, such as the strike-slip faults and the localized thrust faults that likely influenced rock uplift in this area (Liu-Zeng et al., 2008; Tapponnier et al., 2001). We suggest that the gradual propagation in SE Tibet may have been accomplished by southeastward motion of high topography propagating uplift along the strike-slip faults active during the Paleogene. Future work will require other functional forms in time and space enabling better integration of such geologic complexities.

5. Conclusions

Our work provides a new framework to estimate the topographic history of a landscape based on inverse analysis of fluvial erosion-deposition landscape evolution model. The modeling results show that SE Tibet was at low elevation (~300–500 m) and grew outward since 50-25 Ma, and the locus of uplift has continued to propagate toward the southeast as the plateau margin grew outwards. The low Paleogene elevation of SE Tibet and gradual propagating uplift of mountain growth explains the observed river profile morphologies and shape of drainage basins in the plateau margin. Our modeling also precludes the existence of a long period of topographic degradation following the plateau growth. The quantitative constraints on landscape evolution achieved based on drainage patterns in SE Tibet indicate a powerful tool potentially applicable to other regions to infer important implications for the evolution of Indian-Eurasian collision, Asian monsoons, and biodiversity, as well as the geodynamic forces involved in collisional orogens.

Data Availability Statement

The software to conduct the modeling can be found in Yuan et al. (2019), https://doi.org/10.5281/zenodo.3833983 (Bovy & Braun, 2020), NA (Sambridge, 1999), and https://doi.org/10.5281/zenodo.6320495 (Yuan, 2022). Figures were made using ParaView, InkScape, and Python.

Acknowledgments
We are grateful to two anonymous reviewers and Editor Lucy Flesch for the constructive comments. We also thank Jing Liu-Zeng and Kai Cao for the helpful discussions. G.D.-N. acknowledges funding from ERC MAGIC Grant 649081. X.S. acknowledges funding from NSFC Grant 42073052. Glic cluster in GFZ and Goody-1 cluster in CUG were used for the modeling.

References

Botsyun, S., Sepulchre, P., Donnadieu, Y., Risi, C., Licht, A., & Rugenstein, J. K. C. (2019). Revised paleoaltimetry data show low Tibetan Plateau elevation during the Eocene. *Science*, *363*(6430). https://doi.org/10.1126/science.aaq1436

Bouilhol, P., Jagoutz, O., Hanchar, J. M., & Dudas, F. O. (2013). Dating the India-Eurasia collision through arc magmatic records. *Earth and Planetary Science Letters*, *366*, 163–175. https://doi.org/10.1016/j.epsl.2013.01.023

Bovy, B., & Braun, J. (2020). Fastscape-lem/fastscapelib-fortran v2.8.2. *Zenodo*. https://doi.org/10.5281/zenodo.3833983

Clark, M. K., House, M. A., Royden, L. H., Whipple, K. X., Burchfiel, B. C., Zhang, X., & Tang, W. (2005). Late cenozoic uplift of southeastern Tibet. *Geology*, *33*(6), 525–528. https://doi.org/10.1130/g21265.1

Clark, M. K., & Royden, L. H. (2000). Topographic ooze: Building the eastern margin of Tibet by lower crustal flow. *Geology*, *28*(8), 703–706. https://doi.org/10.1130/0091-7613(2000)28<703:tobtem>2.0.co;2

Clark, M. K., Royden, L. H., Whipple, K. X., Burchfiel, B. C., Zhang, X., & Tang, W. (2006). Use of a regional, relict landscape to measure vertical deformation of the eastern Tibetan Plateau. *Journal of Geophysical Research*, *111*, F03002. https://doi.org/10.1029/2005JF000294

DeCelles, P. G., Quade, J., Kapp, P., Fan, M., Dettman, D. L., & Ding, L. (2007). High and dry in central Tibet during the late Oligocene. *Earth and Planetary Science Letters*, *253*(3–4), 389–401. https://doi.org/10.1016/j.epsl.2006.11.001

Deng, T., & Ding, L. (2015). Paleoaltimetry reconstructions of the Tibetan Plateau: Progress and contradictions. *National Science Review*, *2*(4), 417–437. https://doi.org/10.1093/nsr/nwv062

Ding, L., Xu, Q., Yue, Y., Wang, H., Cai, F., & Li, S. (2014). The Andean-type Gangdese mountains: Paleoelevation record from the Paleocene–Eocene Linzhou Basin. *Earth and Planetary Science Letters*, *392*, 250–264. https://doi.org/10.1016/j.epsl.2014.01.045

Ding, W. N., Ree, R. H., Spicer, R. A., & Xing, Y. W. (2020). Ancient orogenic and monsoon-driven assembly of the world's richest temperate alpine flora. *Science*, *369*(6503), 578–581. https://doi.org/10.1126/science.abb4484

Fang, X., Dupont-Nivet, G., Wang, C., Song, C., Meng, Q., Zhang, W., et al. (2020). Revised chronology of central Tibet uplift (Lunpola Basin). *Science Advances*, *6*(50), eaba7298. https://doi.org/10.1126/sciadv.aba7298

Favre, A., Päckert, M., Pauls, S. U., Jähnig, S. C., Uhl, D., Michalak, I., & Muellner-Riehl, A. N. (2015). The role of the uplift of the Qinghai-Tibetan Plateau for the evolution of Tibetan biotas. *Biological Reviews*, *90*(1), 236–253.

Goren, L., Fox, M., & Willett, S. D. (2014). Tectonics from fluvial topography using formal linear inversion: Theory and applications to the Inyo Mountains, California. *Journal of Geophysical Research: Earth Surface*, *119*, 1651–1681. https://doi.org/10.1002/2014JF003079

Gourbet, L., Leloup, P. H., Paquette, J. L., Sorrel, P., Maheo, G., Wang, G., et al. (2017). Reappraisal of the Jianchuan Cenozoic basin stratigraphy and its implications on the SE Tibetan plateau evolution. *Tectonophysics*, *700*, 162–179.

Groves, K., Allen, M., Saville, C., Hurst, M., & Jones, S. (2020). Incision migration across Eastern Tibet controlled by monsoonal climate, not tectonics? *EGU General Assembly Conference Abstracts*. https://doi.org/10.5194/egusphere-egu2020-444

Hetzel, R., Dunkl, I., Haider, V., Strobl, M., vonEynatten, H., Ding, L., & Frei, D. (2011). Peneplain formation in southern Tibet predates the India-Asia collision and plateau uplift. *Geology*, *39*(10), 983–986. https://doi.org/10.1130/g32069.1

Hoke, G. D., Liu-Zeng, J., Hren, M. T., Wissink, G. K., & Garzione, C. N. (2014). Stable isotopes reveal high southeast Tibetan Plateau margin since the Paleogene. *Earth and Planetary Science Letters*, *394*, 270–278. https://doi.org/10.1016/j.epsl.2014.03.007

Jammes, S., & Huismans, R. S. (2012). Structural styles of mountain building: Controls of lithospheric rheologic stratification and extensional inheritance. *Journal of Geophysical Research*, *117*, B10403. https://doi.org/10.1029/2012JB009376

Kapp, P., & DeCelles, P. G. (2019). Mesozoic-Cenozoic geological evolution of the Himalayan-Tibetan orogen and working tectonic hypotheses. *American Journal of Science*, *319*(3), 159–254. https://doi.org/10.2475/03.2019.01

Leloup, P. H., Lacassin, R., Tapponnier, P., Schärer, U., Zhong, D., Liu, X., et al. (1995). The Ailao Shan-Red river shear zone (Yunnan, China), tertiary transform boundary of Indochina. *Tectonophysics*, *251*(1–4), 3–84. https://doi.org/10.1016/0040-1951(95)00070-4

Li, H. A., Dai, J. G., Xu, S. Y., Liu, B. R., Han, X., Wang, Y. N., & Wang, C. S. (2019). The formation and expansion of the eastern Proto-Tibetan Plateau: Insights from low-temperature thermochronology. *Journal of Asian Earth Sciences*, *183*, 103975. https://doi.org/10.1016/j.jseaes.2019.103975

Li, S., Currie, B. S., Rowley, D. B., & Ingalls, M. (2015). Cenozoic paleoaltimetry of the SE margin of the Tibetan Plateau: Constraints on the tectonic evolution of the region. *Earth and Planetary Science Letters*, *432*, 415–424.

Li, Y., Wang, C., Dai, J., Xu, G., Hou, Y., & Li, X. (2015). Propagation of the deformation and growth of the Tibetan-Himalayan orogen: A review. *Earth-Science Reviews*, *143*, 36–61. https://doi.org/10.1016/j.earscirev.2015.01.001

Liu-Zeng, J., Tapponnier, P., Gaudemer, Y., & Ding, L. (2008). Quantifying landscape differences across the Tibetan Plateau: Implications for topographic relief evolution. *Journal of Geophysical Research*, *113*, F04018. https://doi.org/10.1029/2007JF000897

Märki, L., Lupker, M., France-Lanord, C., Lavé, J., Gallen, S., Gajurel, A. P., et al. (2021). An unshakable carbon budget for the Himalaya. *Nature Geoscience*, *14*, 745–750. https://doi.org/10.1038/s41561-021-00815-z

Molnar, P., England, P. C., & Jones, C. H. (2015). Mantle dynamics, isostasy, and the support of high terrain. *Journal of Geophysical Research: Solid Earth*, *120*, 1932–1957. https://doi.org/10.1002/2014JB011724

Penney, C., & Copley, A. (2021). Lateral variations in lower crustal strength control the temporal evolution of mountain ranges: Examples from south-east Tibet. *Geochemistry, Geophysics, Geosystems*, *22*, e2020GC009092. https://doi.org/10.1029/2020GC009092

Perron, J. T., & Royden, L. (2013). An integral approach to bedrock river profile analysis. *Earth Surface Processes and Landforms*, *38*(6), 570–576. https://doi.org/10.1002/esp.3302

Quade, J., Leary, R., Dettinger, M. P., Orme, D., Krupa, A., DeCelles, P. G., et al. (2020). Resetting Southern Tibet: The serious challenge of obtaining primary records of Paleoaltimetry. *Global and Planetary Change*, *191*, 103194. https://doi.org/10.1016/j.gloplacha.2020.103194

Replumaz, A., & Tapponnier, P. (2003). Reconstruction of the deformed collision zone between India and Asia by backward motion of lithospheric blocks. *Journal of Geophysical Research*, *108*(B6), 2285. https://doi.org/10.1029/2001JB000661

Roberts, G. G., & White, N. (2010). Estimating uplift rate histories from river profiles using African examples. *Journal of Geophysical Research*, *115*, B02406. https://doi.org/10.1029/2009JB006692

Rowley, D. B., & Currie, B. S. (2006). Palaeo-altimetry of the late Eocene to Miocene Lunpola Basin, central Tibet. *Nature*, *439*(7077), 677–681. https://doi.org/10.1038/nature04506

Royden, L. H., Burchfiel, B. C., & van der Hilst, R. D. (2008). The geological evolution of the Tibetan Plateau. *Science*, *321*(5892), 1054–1058. https://doi.org/10.1126/science.1155371

Sambridge, M. (1999). Geophysical inversion with a neighbourhood algorithm—I. Searching a parameter space. *Geophysical Journal International*, *138*(2), 479–494. https://doi.org/10.1046/j.1365-246x.1999.00876.x

Shen, X., Braun, J., & Yuan, X. (2022). Southeastern margin of the Tibetan Plateau stopped expanding in the late Miocene. *Earth and Planetary Science Letters*, *583*, 117446. https://doi.org/10.1016/j.epsl.2022.117446

Spicer, R. A., Su, T., Valdes, P. J., Farnsworth, A., Wu, F. X., Shi, G., et al. (2021). Why 'the uplift of the Tibetan Plateau' is a myth. *National Science Review*, *8*(1), nwaa091. https://doi.org/10.1093/nsr/nwaa091

Stock, J. D., & Montgomery, D. R. (1999). Geologic constraints on bedrock river incision using the stream power law. *Journal of Geophysical Research*, *104*(B3), 4983–4993. https://doi.org/10.1029/98JB02139

Su, T., Farnsworth, A., Spicer, R. A., Huang, J., Wu, F. X., Liu, J., et al. (2019). No high Tibetan Plateau until the Neogene. *Science Advances*, *5*(3), eaav2189. https://doi.org/10.1126/sciadv.aav2189

Su, T., Spicer, R. A., Wu, F. X., Farnsworth, A., Huang, J., Del Rio, C., et al. (2020). A Middle Eocene lowland humid subtropical "Shangri-La" ecosystem in central Tibet. *Proceedings of the National Academy of Sciences of the United States of America*, *117*(52), 32989–32995. https://doi.org/10.1073/pnas.2012647117

Tapponnier, P., Zhiqin, X., Roger, F., Meyer, B., Arnaud, N., Wittlinger, G., & Jingsui, Y. (2001). Oblique stepwise rise and growth of the Tibet Plateau. *Science*, *294*(5547), 1671–1677. https://doi.org/10.1126/science.105978

Wang, C., Dai, J., Zhao, X., Li, Y., Graham, S. A., He, D., et al. (2014). Outward-growth of the Tibetan Plateau during the Cenozoic: A review. *Tectonophysics*, *621*, 1–43. https://doi.org/10.1016/j.tecto.2014.01.036

Wei, Y., Zhang, K., Garzione, C. N., Xu, Y., Song, B., & Ji, J. (2016). Low palaeoelevation of the northern Lhasa terrane during late Eocene: Fossil foraminifera and stable isotope evidence from the Gerze Basin. *Scientific Reports*, *6*(1), 27508. https://doi.org/10.1038/srep27508

Whipple, K. X., DiBiase, R. A., Ouimet, W. B., & Forte, A. M. (2017). Preservation or piracy: Diagnosing low-relief, high-elevation surface formation mechanisms. *Geology*, *45*(1), 91–94. https://doi.org/10.1130/g38490.1

Whipple, K. X., & Tucker, G. E. (1999). Dynamics of the stream-power river incision model: Implications for height limits of mountain ranges, landscape response timescales, and research needs. *Journal of Geophysical Research*, *104*(B8), 17661–17674. https://doi.org/10.1029/1999JB900120

Wolf, S. G., Huismans, R. S., Muñoz, J.-A., Curry, M. E., & van der Beek, P. (2021). Growth of collisional orogens from small and cold to large and hot—Inferences from geodynamic models. *Journal of Geophysical Research: Solid Earth*, *126*, e2020JB021168. https://doi.org/10.1029/2020JB021168

Xing, Y., & Ree, R. H. (2017). Uplift-driven diversification in the Hengduan Mountains, a temperate biodiversity hotspot. *Proceedings of the National Academy of Sciences of the United States of America*, *114*(17), E3444–E3451. https://doi.org/10.1073/pnas.1616063114

Xiong, Z., Ding, L., Spicer, R. A., Farnsworth, A., Wang, X., Valdes, P. J., et al. (2020). The early Eocene rise of the Gonjo Basin, SE Tibet: From low desert to high forest. *Earth and Planetary Science Letters*, *543*, 116312. https://doi.org/10.1016/j.epsl.2020.116312

Xiong, Z., Liu, X., Ding, L., Farnsworth, A., Spicer, R. A., Xu, Q., et al. (2022). The rise and demise of the Paleogene central Tibetan valley. *Science Advances*, *8*(6), eabj0944.

Yuan, X. P. (2022). Landscape evolution model and NA. *Zenodo*. https://doi.org/10.5281/zenodo.6320495

Yuan, X. P., Braun, J., Guerit, L., Rouby, D., & Cordonnier, G. (2019). A new efficient method to solve the stream power law model taking into account sediment deposition. *Journal of Geophysical Research: Earth Surface*, *124*, 1346–1365. https://doi.org/10.1029/2018JF004867

Yuan, X. P., Guerit, L., Braun, J., Rouby, D., & Shobe, C. M. (2022). Thickness of fluvial deposits records climate oscillations. *Journal of Geophysical Research: Solid Earth*, *127*, e2021JB023510. https://doi.org/10.1029/2021JB023510

Yuan, X. P., Huppert, K. L., Braun, J., Shen, X., Liu-Zeng, J., Guerit, L., et al. (2021). Propagating uplift controls on high-elevation, low-relief landscape formation in Southeast Tibetan Plateau. *Geology*, *50*, 60–65. https://doi.org/10.1130/G49022.1

Zhao, X., Zhang, H., Hetzel, R., Kirby, E., Duvall, A. R., Whipple, K. X., et al. (2021). Existence of a continental-scale river system in eastern Tibet during the late Cretaceous-early Palaeogene. *Nature Communications*, *12*(1), 7231. https://doi.org/10.1038/s41467-021-27587-9

References From the Supporting Information

Davy, P., & Lague, D. (2009). Fluvial erosion/transport equation of landscape evolution models revisited. *Journal of Geophysical Research*, *114*, F03007. https://doi.org/10.1029/2008JF001146

Guerit, L., Yuan, X. P., Carretier, S., Bonnet, S., Rohais, S., Braun, J., & Rouby, D. (2019). Fluvial landscape evolution controlled by the sediment deposition coefficient: Estimation from experimental and natural landscapes. *Geology*, *47*(9), 853–856.

Howard, A. D., & Kerby, G. (1983). Channel changes in badlands. *Geological Society of America Bulletin*, *94*(6), 739–752.

Kirby, E., & Ouimet, W. (2011). Tectonic geomorphology along the eastern margin of Tibet: Insights into the pattern and processes of active deformation adjacent to the Sichuan Basin. *Geological Society, London, Special Publications*, *353*(1), 165–188.

Liang, S., Gan, W., Shen, C., Xiao, G., Liu, J., Chen, W., et al. (2013). Three-dimensional velocity field of present-day crustal motion of the Tibetan Plateau derived from GPS measurements. *Journal of Geophysical Research: Solid Earth*, *118*, 5722–5732. https://doi.org/10.1002/2013JB010503

Ma, Z., Zhang, H., Wang, Y., Tao, Y., & Li, X. (2020). Inversion of Dadu river bedrock channels for the late Cenozoic uplift history of the eastern Tibetan Plateau. *Geophysical Research Letters*, *47*, e2019GL086882. https://doi.org/10.1029/2019GL086882

Ouimet, W. B., Whipple, K. X., & Granger, D. E. (2009). Beyond threshold hillslopes: Channel adjustment to base-level fall in tectonically active mountain ranges. *Geology*, *37*(7), 579–582.

Replumaz, A., San José, M., Margirier, A., van der Beek, P., Gautheron, C., Leloup, P. H., et al. (2020). Tectonic control on rapid late Miocene—Quaternary incision of the Mekong River Knickzone, southeast Tibetan Plateau. *Tectonics*, *39*, e2019TC005782. https://doi.org/10.1029/2019TC005782

Shobe, C. M., Tucker, G. E., & Barnhart, K. R. (2017). The SPACE 1.0 model: A Landlab component for 2-D calculation of sediment transport, bedrock erosion, and landscape evolution. *Geoscientific Model Development*, *10*(12), 4577–4604.

Yang, R., Fellin, M. G., Herman, F., Willett, S. D., Wang, W., & Maden, C. (2016). Spatial and temporal pattern of erosion in the three rivers region, southeastern Tibet. *Earth and Planetary Science Letters*, *433*, 10–20.

Yang, R., Willett, S. D., & Goren, L. (2015). In situ low-relief landscape formation as a result of river network disruption. *Nature*, *520*(7548), 526–529.